Tribol Lett
DOI 10.1007/s11249-013-0195-x

ORIGINAL PAPER

Mechanism of Action of WS_2 Lubricant Nanoadditives in High-Pressure Contacts

Monica Ratoi · Vlad Bogdan Niste · John Walker · Jurgita Zekonyte

Received: 2 July 2013 / Accepted: 30 July 2013

Abstract Because of their excellent tribological properties and potential to replace problematic lubricant additives currently in use, WS_2 nanoparticles have spurred considerable interest over the last two decades from academia and industry to decipher their mechanism of action. To elucidate the mechanism, this study carried out tribological tests at low and high temperatures and investigated the wear track and friction properties. It was found that in high-pressure, high-temperature sliding contacts, WS_2 nanoadditives react with the metal substrate to generate thick chemical tribofilms which account for their excellent tribological properties. Based on XPS and FIB/SIMS results, a layered structure was proposed for the chemically formed tribofilms. The large amount of W in the composition of the reacted tribofilm could explain the excellent mechanical and antiwear properties, while the exfoliated squashed WS_2 NPs which fill the gaps and cover the reacted tribofilm account for the striking reduction in the boundary friction.

Keywords WS_2 nanoparticles · Mechanism of action · Tribofilm · Composition · Hardness · Friction modifiers · Antiwear additives

1 Introduction

Nanoparticles are very attractive novel lubricant additives because of their nanoscale size, which allows them to penetrate contacts of diverse geometries, fill the gaps between contact asperities and ultimately form a protective boundary film, persistent under high pressure. For this reason, a vast array of nanoparticles has been used in published research to investigate their effect on friction or wear in tribological contacts [1–5].

Tungsten disulphide nanoparticles (WS_2 NPs) have received particular interest because, apart from being highly effective in reducing friction and wear between moving parts [6–12], they are inert, non-toxic, non-magnetic and have high resistance to oxidation and thermal degradation [13]. Their positive influence is especially visible in mixed or boundary lubrication regimes [14] when the most severe wear and damage occur.

WS_2 NPs have a multi-layered structure and exist in two forms: 2H and IF (inorganic fullerene-like). In 2H-WS_2, the layers are flat and present 'dangling bonds'(edge effects that cause deterioration of the nanoparticle through oxidation or burnishing) [6], while in IF-WS_2 NPs, the layers are rounded up to form closed, 'onion-like' cages [15]. In the latter, the edge effects are no longer present and the particles are more inert to chemicals. From the tribological point of view, it has been reported that under high PV (load × velocity) conditions, as encountered in most engineering applications, 2H-WS_2 outperform IF-WS_2 NPs, while in relatively low PV, IF are better [16]. Manufacturing IF-WS_2 NPs involves higher temperatures and also reduces their availability to functionalization. For these reasons, 2H-WS_2 NPs could be more convenient to employ as lubricant nanoadditives in high-pressure tribological applications.

Electronic supplementary material The online version of this article (doi:10.1007/s11249-013-0195-x) contains supplementary material, which is available to authorized users.

M. Ratoi (✉) · V. B. Niste · J. Walker · J. Zekonyte
National Centre for Advanced Tribology, University of Southampton, Southampton, UK
e-mail: m.ratoi@soton.ac.uk

Published online: 21 August 2013

A large number of research studies have attempted to explain the mechanism of action of WS_2 NPs by proposing many hypotheses [16–22]. During the last 20 years, the attention has focused on IF-WS_2 NPs, and their mechanism of action has been studied in numerous publications.

Because IF and 2H-WS_2 NPs possess a layered morphology similar to graphite and other transition metal dichalcogenides (such as MoS_2) which exfoliate under shear and in this way reduce friction, most studies have investigated their ability to behave in the same way. Techniques such as TEM and Raman analysis were employed to show that delaminated 2H-WS_2 sheets adhere to the wear track to form a tribofilm [18, 20, 21] and ascribed their superior tribological properties to this mechanism of action. However, this mechanism can only explain the friction-reducing properties of WS_2 NPs and not their excellent antiwear properties, effective over a wide range of loads.

Another attempt to explain the friction-reducing mechanism of WS_2 NPs was ascribed to the general ability of NPs to fill the asperity valleys of the contact surfaces due to their nanosize. The authors concluded that in order to be effective, NPs have to be smaller than the asperities and the gap between the contacting surfaces [19]. However, this condition implies that IF-WS_2 NPs with an average size of 120 nm, as used in these studies, cannot be effective in the boundary and even mixed lubrication regimes, where the gaps are usually smaller than 100 nm.

In the case of IF-WS_2 NPs, one of the first attempts to explain the mechanism of action stipulated their potential to act as rolling nano ball bearings. Under low loads, the shear force between the inner and outer closed layers of the NPs was not considered to be high enough to exfoliate them, as in the case of the flat layered structures, such as graphite and transition metal dichalcogenides [16]. This hypothesis was investigated by Golan [23] who used multiple-beam interferometry in the surface force apparatus to show that there was no evidence for 'rolling friction,' and the low values of the coefficient of friction (COF) can be explained by the friction-induced transfer layers of WS_2 to the lubricated contact surfaces. However, some recent studies [21, 22], which investigated the rolling mechanism of IF NPs in HRSEM and TEM-AFM in high- and, respectively, low-pressure contacts showed that well crystallized, spherically shaped IF NPs can reduce friction through a rolling mechanism. These studies were carried out on atomically smooth silica wafers [21], and the question arises whether in real contact conditions, in which nanoparticles could get trapped or jammed between the surface asperities, the rolling motion is still enabled.

Two studies investigated the boundary lubrication mechanism of IF-WS_2 NPs coated with trioctylamine and methyltrioctylammoniumchloride (200 nm diameter) under high loads at 25 °C [10, 11]. The authors claimed that the mechanism may be ascribed to a tribochemical reaction film, but their X-ray photoelectron spectroscopy (XPS) data of the wear tracks only shows the presence of Fe, C, O and N (from the functionalization groups). Another study, which also used XPS analysis to investigate the wear track generated by WS_2 NPs at room temperature, found small concentrations of tungsten oxide (1.4 at.%), tungsten sulphide and iron oxides [18].

Most investigations of the tribological properties of WS_2 NPs have been carried out at room temperature, except for two studies which tested the NPs at 75 [14] and 80 °C, respectively [24]. However, the authors did not report the presence of a tribofilm on the wear track.

This study aims to elucidate the mechanism of action of WS_2 NPs in high-pressure contacts by investigating the tribofilm generation on the wear track in a ball-on-disc set-up throughout a range of testing temperatures and lubrication regimes. The chemical composition of the tribofilms was investigated with XPS and secondary ion mass spectroscopy (SIMS), and the results from the chemical tests were compared with the mechanical properties derived from nanoindentation tests.

2 Results and Discussion

2.1 WS_2 Nanoadditive Characterization

WS_2 NPs were purchased from MK Impex Corporation and characterized using X-ray powder diffractometry (XRD), Raman spectroscopy, transmission electron microscopy (TEM) and energy-dispersive X-ray spectroscopy (EDX; see Supporting Information). The particle size distribution of WS_2 NP dispersions in oils was measured by dynamic light scattering. The results showed that the WS_2 NPs were not fullerene-like, but flat, stacked sheets of 2H-WS_2.

The XRD pattern (Fig. 1) shows that all the diffraction peaks are indexed to hexagonal WS_2. As reported in the literature, all the peaks are sharp, especially (002) and (101)—as opposed to those of IF-WS_2, which are broadened due to the small crystal size [25, 26].

Furthermore, the (002), (004) and (006) peaks are much stronger than expected from JCPD standards due to the preferential orientation of the flat sheets (Fig. 2).

The Raman scattering spectrum for WS_2 is shown in Fig. 3. Two signals are present at 355 and 419 cm^{-1}, consistent with other published research values for the E^1_{2g} and A_{1g} bands [9, 20, 25–27]. The A_{1g} peak represents the S–S vibration between two different layers (inset in Fig. 3). The relative intensity of the A_{1g} peak suggests that the vibration energy is small and that the nanoparticles therefore contain only a few stacked layers [26].

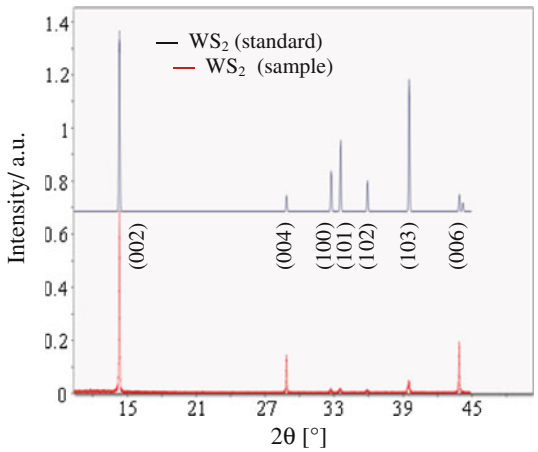

Fig. 1 XRD diffraction pattern of 2H-WS_2 NPs

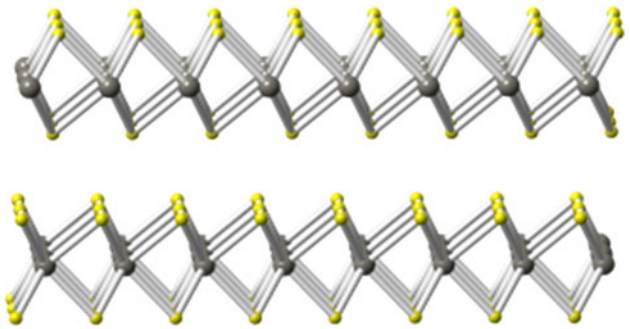

Fig. 2 Structure and orientation of 2H-WS_2 layers

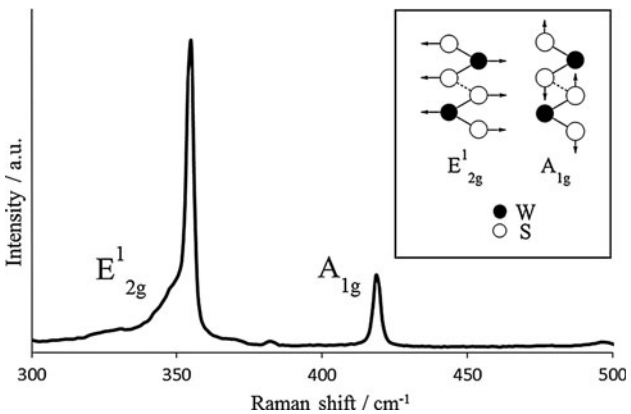

Fig. 3 Raman spectrum of WS_2 NPs

The shape and morphology of the NPs were investigated using transmission electron microscopy. The TEM pictures shown in Fig. 4 suggest the presence of two populations of WS_2 NPs of distinct morphologies (Fig. 4a). The trigonal prismatic geometry of the 2H-WS_2 crystal structure is reflected in the triangular and hexagonal shapes of the NPs (Fig. 4b–d).

This particular size distribution could be beneficial for tribological applications, conferring the nanoadditive the ability to penetrate contacts and fill asperity gaps of different sizes in order to limit the adhesion of contact surfaces and ultimately reduce friction.

EDX analysis showed WS_2 NPs contain only tungsten and sulphur (see Supporting Information).

2H-WS_2 NP dispersions in base oil (a polyalphaolefin, Mobil SpectraSyn Plus 6) with a concentration of 1 wt% were prepared using a probe sonifier. This concentration was recommended in published research as optimal for tribological applications [14]. To avoid any competition for the additive to adhere/adsorb/react on the lubricated metal surface, the base oil was specifically chosen to have a very low polarity (as is the case of PAOs), and no surfactant/dispersant was used to stabilize the dispersions. The PAO base oil has a density of 830 kg/m^3 at 15 °C and viscosity of 30.3 cSt at 40 °C and 5.9 cSt at 100 °C.

The size distribution of the WS_2 NPs dispersed in PAO was measured with the Malvern Zetasizer immediately after preparation. The intensity distribution, as shown in Fig. 5, shows two narrow peaks (which indicate that the NPs were monodispersed) and the presence of two distinct size NP populations: one with an average size of 30–40 nm and the other of approximately 250 nm.

2.2 WS_2 Nanoadditive Tribological Performance

Tribological tests were carried out on a mini traction machine (MTM2) in a sliding-rolling ball-on-disc set-up which features a 19-mm-diameter ball and a 46-mm-diameter disc, both made of AISI 52100 steel (hardness 750–770 HV). The root-mean-square roughness of both balls and discs is 11 ± 3 nm, resulting in a composite surface roughness of approximately 16 nm. New specimens (balls and discs) were used for each test and were cleaned with solvents in an ultrasonic bath for 10 min prior to the test. Throughout the test, the temperature was kept constant (40 and 100 °C, respectively) and the applied load was 30 N, corresponding to an initial mean Hertz pressure of 0.94 GPa. The slide-roll ratio, calculated as the ratio of the sliding speed $|u_b - u_d|$ to the entrainment speed $(u_b + u_d)/2$ (where u_b and u_d are the speed of the ball and the disc, with respect to the contact) was 150 %. This slide-roll ratio value was selected to be higher than in previously reported research [28] to accelerate the generation of the chemically reacted tribofilm, which is known to depend on the severity of the rubbing conditions [29]. During the test, the NP dispersion was maintained at constant temperature in the enclosed, temperature-insulated chamber, where it was stirred continuously and vigorously by the circular movements of the disc and ball. Therefore, even in the absence of a surfactant, NPs were maintained well dispersed and only a small number sedimented at the bottom of the lubricant chamber at the end of the 3-h test.

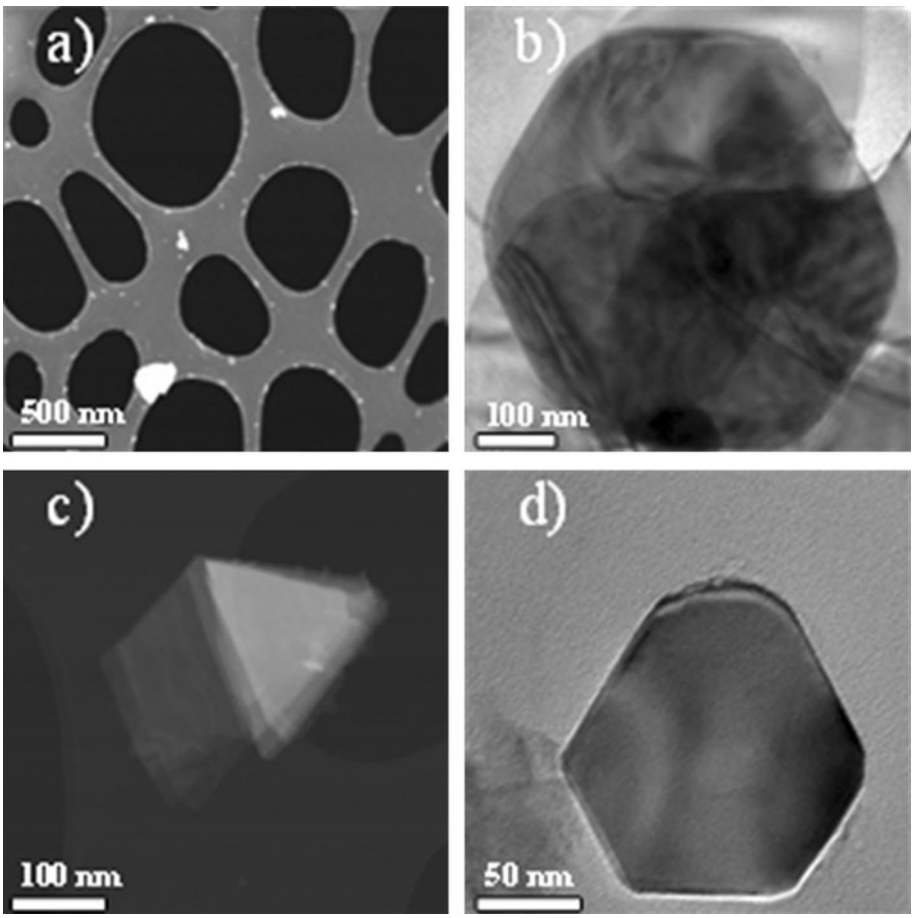

Fig. 4 TEM pictures showing **a** the two 2H-WS_2 nanoparticle populations; **b–d** 2H-WS_2 (*plate*-like) nanoparticles

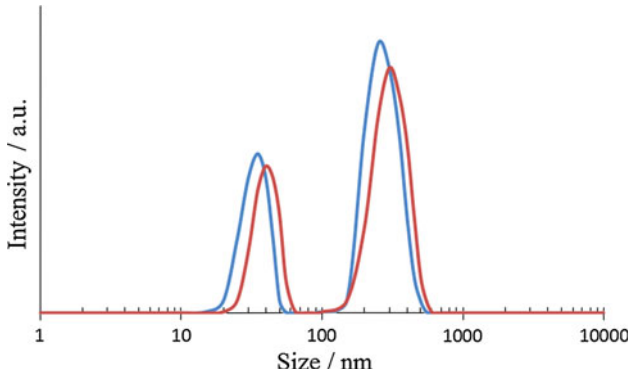

Fig. 5 Size distribution for 1 wt% 2H-WS_2 NPs in PAO

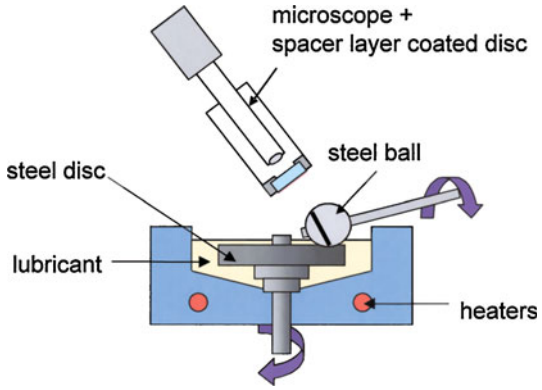

Fig. 6 Diagram of MTM2-SLIM set-up [30]

The MTM2 is fitted with the 3D spacer layer imaging method (SLIM) attachment, which enables in situ capture of optical interference images of the tribofilms on the steel ball (Fig. 6). These are used to calculate the thickness of the tribofilm generated during the test.

The tribological tests followed a routine which can be divided in three alternative stages repeated at fixed time intervals. The first stage was the 'conditioning phase', when the ball and disc were rubbed together at a fixed slow entrainment speed in mixed lubrication film conditions to generate a tribofilm on the ball and disc wear track. The following stage consisted of the 'Stribeck curve' acquisition, in which friction was measured over a range of entrainment speeds at a fixed slide-roll ratio. The acquisition of data for the Stribeck curve started at the highest speed (1.5 m/s) and continued towards the lowest speed (10 mm/s) value to protect the formed tribofilm by avoiding its damage at low speeds in the boundary regime. The third stage was the 'tribofilm measurement'; when the motion was halted, the spacer layer-coated window was

loaded against the ball track and an image was captured. The conditions used for the MTM2-SLIM tests in this study are summarized in Table 1.

Figures 7 and 8 show the variation of the COF with speed (Stribeck curves) for WS_2 NP dispersions in PAO, at 40 and 100 °C after 1, 10, 30, 90 and 180 min of rubbing in the 'conditioning phase' at 100 mm/s (in mixed lubrication regime).

The Stribeck curves for the dispersion tested at 40 °C (Fig. 7) show an almost linear increase in friction with decreasing speed in all the lubrication regimes throughout the experiment. The boundary COF increased with rubbing time from 0.09 (after 1 min) to 0.11 (after 180 min).

At 100 °C (Fig. 8), all Stribeck curves show a similar pattern throughout the test. As the speed decreases from 1.5 m/s to 100 mm/s in the mixed lubrication regime, the curves reach a peak COF value at the end of the mixed lubrication regime (100 mm/s), followed by a sharp and constant decrease all the way into the boundary regime (100–10 mm/s). However, as the test progressed with time, the Stribeck curves shifted upward towards higher values of COF. The highest COF value of 0.09 was reached after 90 min of rubbing and remained constant until the end of the 3-h test. This behaviour has been previously reported for the zinc dithiophosphate (ZDDP) antiwear additives tested under similar conditions, when a rough tribofilm of considerable thickness formed on the wear track [31]. The antiwear films formed by ZDDP have high boundary friction coefficients in the range of 0.11–0.14, which are maintained up to much higher sliding speeds than is normally the case. The high boundary friction of the ZDDP tribofilms is thought to be due to their unusual morphology. In order to reduce the friction, it is especially important to use efficient friction modifiers along with ZDDPs when formulating lubricants.

The sharp decrease in the COF values to 0.05–0.06 at low rolling speeds and the maintenance of this value for the rest of the test period is reminiscent of the behaviour of some of the most efficient friction modifiers [32].

Table 1 MTM2—SLIM test conditions

Conditioning phase	
Temperature	40 °C, 100 °C
Load	30 N
Mean Hertz pressure	0.94 GPa
Entrainment speed	0.1 m/s
Slide-roll ratio	150 %
Stribeck curve phase	
Temperature	40 °C, 100 °C
Load	30 N
Mean Hertz pressure	0.94 GPa
Entrainment speed	1.5–0.01 m/s
Slide-roll ratio	150 %

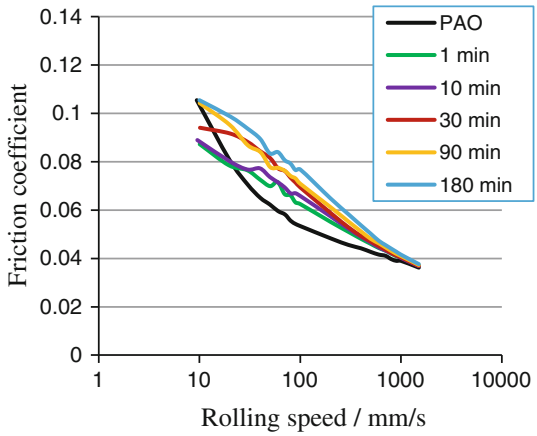

Fig. 7 Stribeck curves for 1 wt% WS_2 NPs in PAO at 40 °C after 1, 10, 30, 90 and 180 min of rubbing

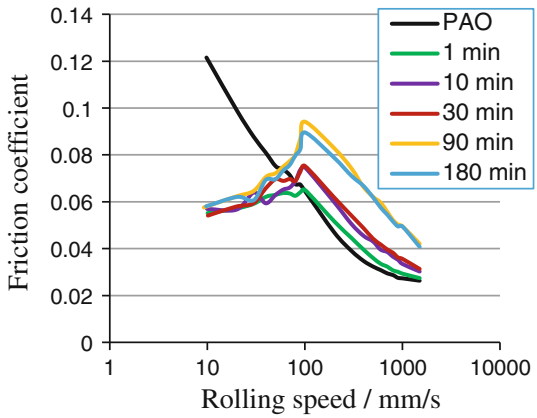

Fig. 8 Stribeck curves for 1 wt% WS_2 NPs in PAO at 100 °C after 1, 10, 30, 90 and 180 min of rubbing

2.3 Characterization of WS_2 Nanoadditive Tribofilm

The striking difference between the Stribeck curves of the WS_2 NP dispersions measured at 40 and 100 °C suggests that the mechanism of action is different in each case and that temperature plays a key role. To understand the reason behind the different behaviour and the mechanism of action of WS_2 nanoadditives, a study of the physical, chemical and micromechanical characteristics of the tribofilm generated on the wear track was considered paramount.

For the physical characterization of the tribofilm (thickness, distribution and roughness), three techniques were employed: 3D SLIM interference, optical microscopy and Alicona profilometry.

Figures 9 and 10 show images of the ball and disc wear tracks obtained with the WS_2 NP dispersions in PAO at 40 and 100 °C. Thickness profiles of the wear tracks were

Fig. 9 Images of the tribofilm generated at 40 °C after the 3-h conditioning time **a** optical image of the wear track on the *disc*; **b** Alicona 3D optical image of the tribofilm on the *disc*; **c** 3D SLIM interference image of the tribofilm on the *ball*

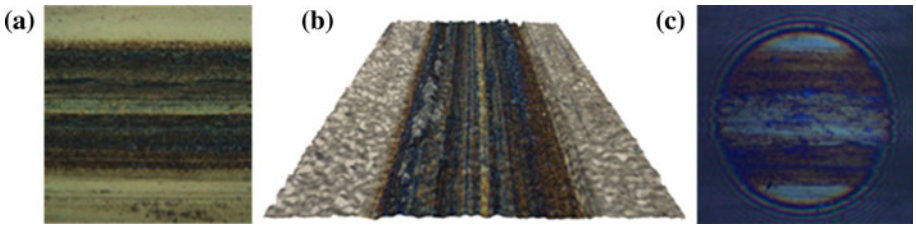

Fig. 10 Images of the tribofilm generated at 100 °C after the 3-h conditioning time **a** optical image of the wear track on the *disc*; **b** Alicona 3D optical image of the tribofilm on the *disc*; **c** 3D SLIM interference image of the tribofilm on the *ball*

measured before and after the 3-h tests with the alicona infinite focus profilometer, at 20× magnification.

The wear track generated at 40 °C (Fig. 9) showed a thin, patchy tribofilm (30 nm) which displayed local NP agglomerations. A more uniform tribofilm with an average thickness of 100 nm (as measured with 3D SLIM and Alicona) was generated at 100 °C (Fig. 10; Table 2).

The chemical composition of the tribofilms was investigated with XPS and secondary ion mass spectroscopy (SIMS).

XPS with depth profiling sputtering was employed to study the elemental composition and chemical state of elements in the tribofilm layers. The depth profile also showed how the chemical state of the monitored elements changes through the layers.

On the wear track generated at 40 °C, the XPS analysis was performed on an area with fewer NP agglomerations. The results (Table 3) show small quantities of tungsten in the form of W^{6+} (such as in WO_3) and sulphur in the form of iron sulphide. These indicate that a reaction started to take place between the steel substrate and the NPs, but the temperature was unfavourable. After etching, only iron, oxygen and carbon were detected (most likely from iron oxides and oxidized residues of oil molecules).

In the tribofilm generated at 100 °C, carbon was found on the surface, probably due to the degradation of the oil. Otherwise, the presence of oxygen, sulphur, iron and tungsten was detected (Fig. 11). From the tribofilm thickness measurements, the final total etched depth was estimated to be 200 nm.

A large amount of W is found throughout the depth of the tribofilm. Sulphur is also present in the top 50 nm, as part of unreacted WS_2 NPs and iron sulphides. Iron is in the form of iron sulphides and oxides (near the surface) and elemental iron.

Core level spectra for W in WS_2 were recorded at binding energies of 33.2 eV but were only found as traces (Fig. 12). The main signals are for W^{6+}, specific to WO_3 (35.6 eV) and for W^0 (31.2 eV) [25, 33, 34]. The only exception was in the unsputtered layer, where W was found at 31.5 eV. The shift of ~0.3 eV between the non-sputtered and sputtered layers is generally due to a slight energy loss of the electrons coming through the carbon contamination layer on top.

The XPS results of the tribofilms generated at the two temperatures (but otherwise identical testing conditions) prove that the tribofilms are generated through a chemical reaction between the WS_2 nanoadditive and the metal substrate, and the temperature plays a major role in this process. A similar mechanism of action is known to occur in the case of antiwear or extreme pressure additives (e.g. ZDDP) [28].

To acquire extra information about the thickness, morphology and chemistry of the tribofilms generated under the two temperature conditions, scanning electron microscopy (SEM) with focused ion beam (FIB) and secondary ion mass spectroscopy (SIMS) analysis (Fig. 13) were carried out.

The SEM pictures of the wear track generated at 40 °C showed some non-uniformly distributed deposits of NPs (Fig. 13a). The wear track generated at 100 °C was imaged in a thicker region than average. In this specific position (Fig. 13b–d), the track was uniformly covered by a 200-nm-thick chemically formed tribofilm.

Table 2 Tribofilm thickness measured using Alicona profilometry and SLIM

	40 °C	100 °C
Measured values of tribofilm thickness (nm)		
Alicona	37	109
SLIM	26	98

Table 3 XPS results: composition of the tribofilm formed at 40 °C before etching

	W 4f	S 2p	Fe 2p	O 1s	C 1s
Comp (%)	0.1	1.1	26	37.1	35.7

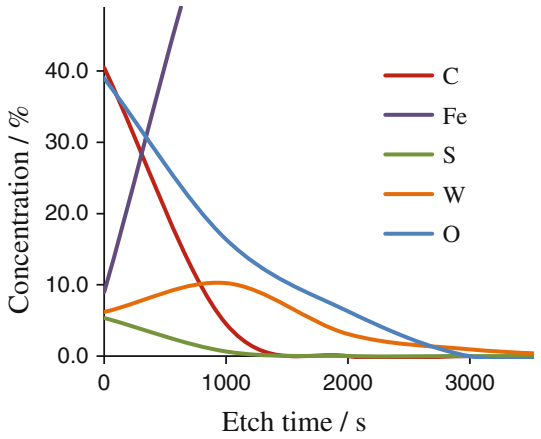

Fig. 11 Depth profile of the tribofilm generated at 100 °C using XPS

Secondary ion mass spectroscopy (SIMS) was also employed to reveal the chemical composition of the tribofilms and to map its layers. The SIMS depth profiling of the tribofilm generated at 100 °C (Fig. 14) monitored the variation in chemical composition of different layers as the FIB etched deeper into the tribofilm.

Aside from the chemical composition of the tribofilm which was found to be similar to the XPS results, the SIMS data also offer valuable information on the arrangement of layers with different chemistry. The tribofilm was found to contain tungsten below a sulphur-rich layer. This arrangement suggests that the upper part of the tribofilm contains tungsten and iron sulphides, while at the interface with the steel substrate, it is composed of tungsten and iron, in their oxide and elemental states.

The XPS and SIMS results for the tribofilm generated at 100 °C indicate that it is likely to be formed of several layers as illustrated in Fig. 15:

- carbon impurities and unreacted sheets of WS_2 on the surface
- a layer of WO_3, iron oxides and sulphides, elemental Fe and W

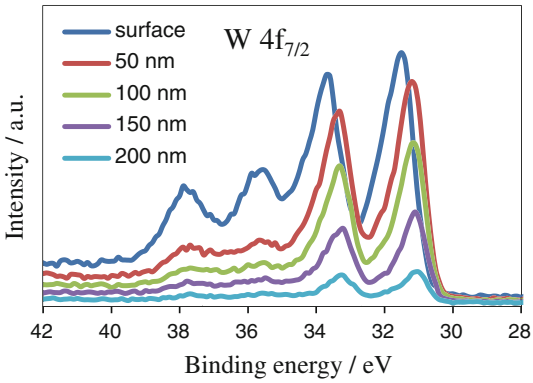

Fig. 12 XPS spectra zoomed on the W energy region

- a layer WO_3, elemental Fe and W
- a layer of elemental Fe and W

The results from the chemical analysis confirm that the tribofilm was generated by a chemical reaction between the WS_2 NPs and the steel substrate, controlled by temperature. The chemical tribofilm could account for the excellent antiwear properties of WS_2 NPs reported in the published research. A similar mechanism of action is reported in the case of antiwear (e.g. ZDDP) and extreme pressure additives [28]. However, the ZDDP antiwear films are known to increase the boundary friction, while the tribofilms generated by WS_2 NPs show very low friction levels, similar to the friction modifiers. The strikingly different friction properties of tribofilms generated by ZDDPs and WS_2 NPs could be attributed to the dissimilar morphology or micromechanical properties of the tribofilm. To investigate these properties, visualization and nanoindentation tests were conducted on the tribofilms generated by WS_2 NPs at 100 °C.

Nanoindentation is a depth-sensing technique capable of providing measurements of elastic and plastic properties, where the indentation process is continually monitored with respect to force, displacement and time. Nanoindentation of tribofilms was performed using a pendulum-based NanoTest Platform 3 instrument (Micro Materials, Wrexham, UK) [35].

Indentations were performed using a Berkovich diamond indenter in a depth-controlled mode. Maximum penetration depth was set to 30 nm, the maximum loading force was 1 mN, loading and unloading rates were kept constant, with loading and unloading times set to 20 s, and a dwell time of 10 s was selected at maximum load to reduce the influence of creep. A matrix of 100 indents was imprinted onto the sample surface (15 μm apart, over an area of 150×150 μm^2) to map the distribution of mechanical properties. The data were analysed using the Oliver and Pharr method with the analytical software provided by manufacturers with the instrument. Hardness and reduced elastic modulus were determined [36].

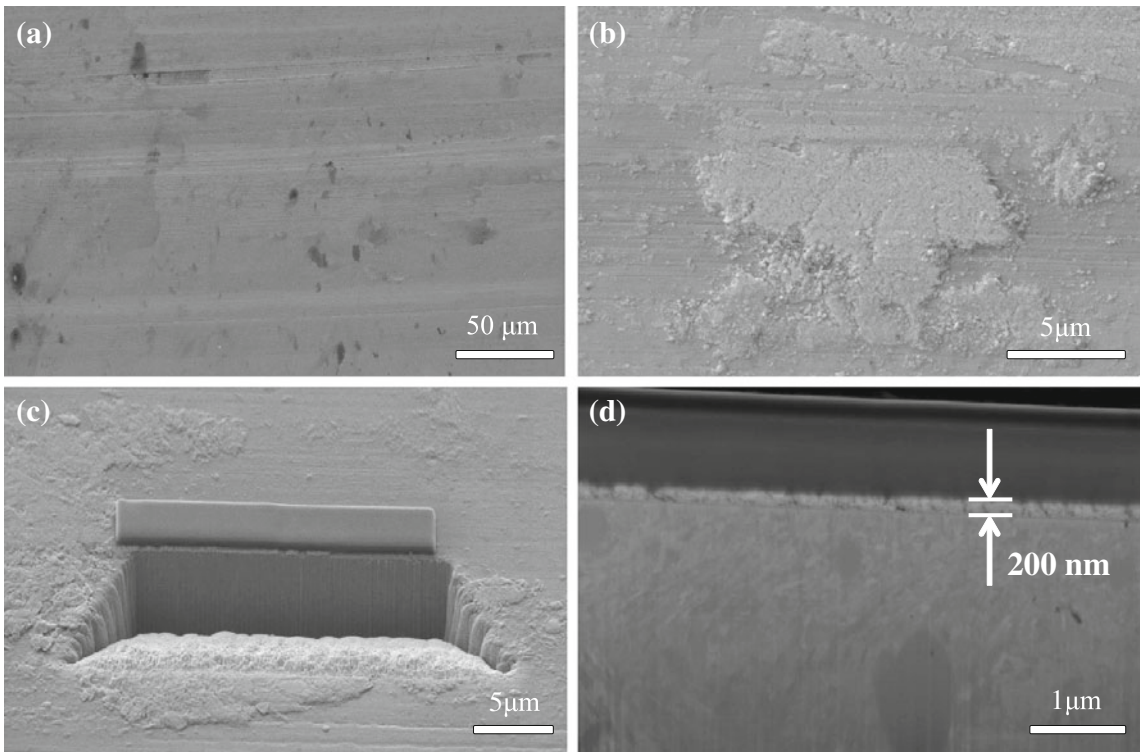

Fig. 13 **a** SEM picture of the wear track generated at 40 °C, displaying a few NP agglomerations; **b** SEM picture of the wear track generated at 100 °C, covered by a tribofilm; **c** SEM picture taken during the analysis of wear track generated at 100 °C; **d** Profile view of the tribofilm formed by the PAO NP dispersion on the track at 100 °C

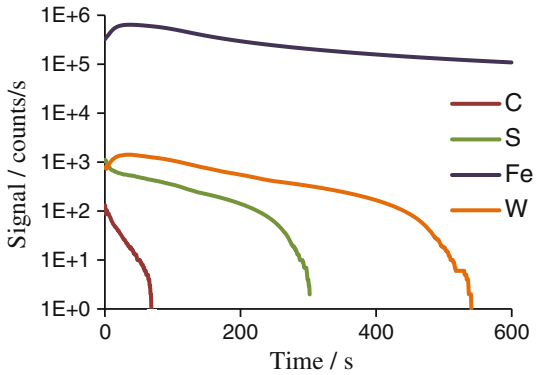

Fig. 14 Depth profile of the tribofilm generated at 100 °C using SIMS

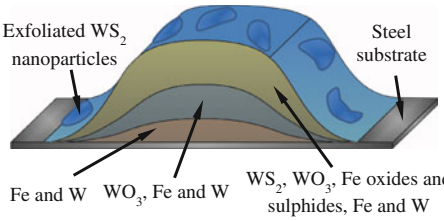

Fig. 15 Likely composition of the tribofilm generated by WS_2 NPs at 100 °C

Nanoindentation tests of the steel substrate were also performed outside the wear track for comparison reasons. As shown in Fig. 16, the analysis was started from outside the tribofilm moving towards its centre, as follows: section (1)—steel; section (2)—chemically formed tribofilm; section (3)—chemically formed tribofilm covered with a thick layer of unreacted, squashed WS_2 NPs and section (4)—chemically formed tribofilm with a few NPs.

The hardness (H) and reduced Young's modulus (E_r) values measured in the four sections (on steel and tribofilm) are shown in Table 4.

Sections 2, 3 and 4 found on the tribofilm show different values of the two parameters. In sections 3 and 4, the hardness and reduced Young's modulus also have a high standard deviation because, as shown in Fig. 16, the tests were performed on chemically reacted layers which were covered with NPs.

To reduce the influence of the steel substrate, the nanoindentation analysis was performed on the thickest part of the tribofilm, where the measured chemical tribofilm was approximately 200 nm. The average thickness of unreacted NP layer found on top of the chemical tribofilm was measured with the alicona infinite focus to be 250 nm (Fig. 17). Therefore, the indention in section 3 is carried out only through the layer of squashed NPs and was not influenced by the chemically formed tribofilm. The

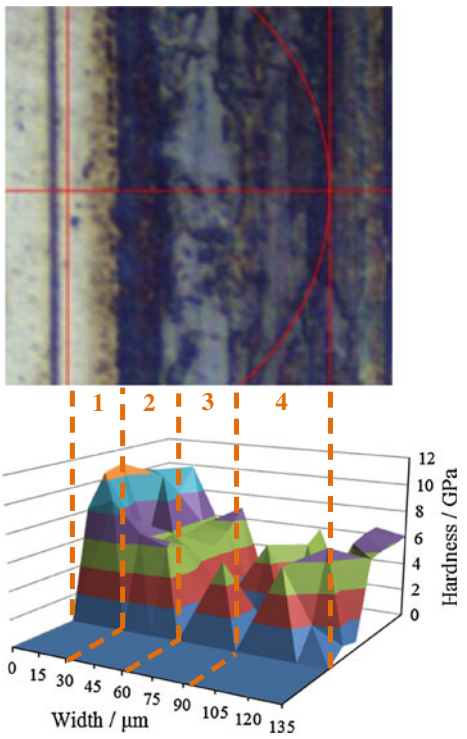

Fig. 16 Map of nanoindented sections of steel and tribofilm (points are 15 µm apart)

Table 4 Measured values for H and E_r in the four sections (steel and tribofilm)

	Section	Mechanical parameters (GPa)	
		H	E_r
1	Steel	8.9 ± 1.6	192.5 ± 17.3
2	Tribofilm	5.7 ± 0.7	165.5 ± 17.1
3	Tribofilm fully covered with NPs	1.9 ± 1.9	92.4 ± 45.8
4	Tribofilm with a few NPs	4.5 ± 2.5	132 ± 50

squashed NPs and the chemical tribofilm have very distinctive values of mechanical parameters measured which can be separated as shown in Table 5.

The force–distance curves shown in Fig. 18 indicate that the behaviour of the squashed layer of WS_2 NPs is markedly different. During the 10-s dwell time at maximum load, the soft NP structure was penetrated to a large depth while no major elastic behaviour was noticed during the unloading.

The hardness and reduced Young's modulus values of the WS_2 tribofilm are higher than those reported for tribofilms generated by other oil additives ($H = 5$ GPa and $E_r = 110$ GPa for ZDDP [37]; $H = 0.4$ GPa and $E_r = 10$ GPa for MoDTC [38]). These values indicate that the presence of tungsten in tribofilms improves their mechanical properties and consequently improves the

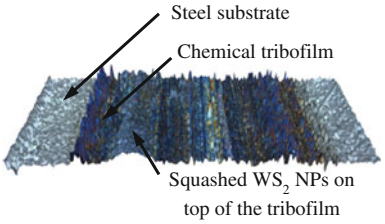

Fig. 17 Alicona profile view across the tribofilm

Table 5 H and E_r values for the chemical tribofilm and squashed WS_2 NPs

	H (GPa)	E_r (GPa)
Tribofilm	5.8 ± 0.6	165.7 ± 19.4
Squashed NPs	1 ± 0.4	72.7 ± 24.8

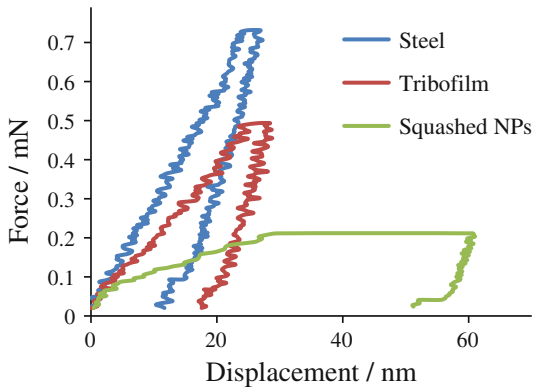

Fig. 18 Loading/unloading hysteresis on the three different types of substrate

antiwear behaviour. Therefore, the ability of WS_2 NPs to generate chemically reacted tribofilms on the wear track can explain the excellent antiwear behaviour reported by many studies for this nanoadditive. These thick and patchy chemical tribofilms are similar to those generated by ZDDP antiwear additive, but they are covered with platelet-like 2H-WS_2 NPs, which have the effect of levelling and smoothing the rough areas and therefore of reducing boundary friction.

3 Conclusions

Previously published work showed that 2H and IF WS_2 NPs are strong candidates to replace environmentally harmful lubricant additives because of their potential to reduce friction and wear in high-pressure contacts. The research was mainly carried out at room temperature, and the mechanism of action proposed was the delamination of NPs under pressure and adherence of WS_2 sheets to the

wear track to generate a tribofilm. However, this mechanism can only explain its friction-reducing ability but not the antiwear properties.

This study has employed WS_2 NPs from MK IMPEX Corp., Canada, which were characterized with XRD, Raman, TEM and EDX, and found to be 2H-WS_2 NPs. 1 wt% WS_2 NP dispersions in PAO were prepared and their dispersion state and tribological properties were assessed.

The ability of 2H-WS_2 NPs to reduce boundary friction in high-pressure sliding contacts was found to be largely dependent on temperature.

WS_2 NP dispersions tested at 40 °C displayed a modest reduction in boundary friction which was gradually lost as the test progressed with time. The optical and XPS analysis of the wear track showed the generation of an irregular tribofilm with a thickness of approximately 30 nm, composed of WS_2 sheets or squashed NPs. The small quantities of WO_3 and iron sulphides detected in the tribofilm indicate that a chemical reaction started to take place between the steel substrate and the 2H-WS_2 NPs, but this was not temperature favoured.

At 100 °C, the NP dispersions immediately exhibited a significant reduction in COF in the boundary regime to values of 0.05–0.06 and a gradual, time-dependant increase in friction in the mixed regime. During the conditioning (rubbing) phase of the test, a uniform tribofilm was generated on the wear track. Chemical analysis has indicated that the nanoadditive reacts with the metal substrate and forms a chemical tribofilm with a thickness of 100–200 nm. The chemical composition of the tribofilm was investigated with XPS and SIMS and found to have a layered structure. The upper part of the tribofilms are formed of unreacted WS_2 sheets and/or squashed WS_2 NPs, WO_3, iron oxides and sulphides. The deeper layers consist of WO_3 and elemental W and Fe, while the interface with the steel substrate is composed of only elemental W and Fe. The chemical composition of the tribofilm explains its high hardness (5.8 ± 0.6 GPa) and reduced Young's modulus (166 ± 19 GPa) values and the excellent antiwear properties reported by previously published research.

The chemical tribofilms generated by WS_2 NPs have a thickness and morphology similar to those generated by ZDDP antiwear additives. However, in the case of 2H-WS_2, exfoliated and squashed NPs fill the gaps and cover the reacted tribofilm exerting a levelling and smoothing effect which reduces boundary friction to the levels attained by the best performing friction modifiers.

2H-WS_2 NPs have the advantage of reducing both friction and wear in high-pressure sliding contacts and show great potential for the replacement of some of the most popular but problematic additives in use.

Acknowledgments The authors wish to acknowledge Ian MacLaren from Glasgow University for the TEM analysis, Dr Benjamin Johnson from Leeds University for the XPS analysis, Southampton Nanofabrication Centre for the FIB-SIMS analysis and EPSRC for funding these investigations.

Conflict of interest The authors declare no competing financial interest.

References

1. Bakunin, V.N., Suslov, A.Y., Kuzmina, G.N., Parenago, O.P.: Synthesis and application of inorganic nanoparticles as lubricant components—a review. J. Nanopart. Res. **6**(2), 273–284 (2004). doi:10.1023/B:NANO.0000034720.79452.e3
2. Rozenberg, B.A., Tenne, R.: Polymer-assisted fabrication of nanoparticles and nanocomposites. Prog. Polym. Sci. **33**(1), 40–112 (2008). doi:10.1016/j.progpolymsci.2007.07.004
3. Wu, Y.Y., Tsui, W.C., Liu, T.C.: Experimental analysis of tribological properties of lubricating oils with nanoparticle additives. Wear **262**(7–8), 819–825 (2007). doi:10.1016/j.wear.2006.08.021
4. Zhang, M., Wang, X., Fu, X., Xia, Y.: Performance and anti-wear mechanism of $CaCO_3$ nanoparticles as a green additive in poly-alpha-olefin. Tribol. Int. **42**(7), 1029–1039 (2009). doi:10.1016/j.triboint.2009.02.012
5. Hernandez Battez, A., Gonzalez, R., Viesca, J.L., Fernandez, J.E., Diaz Fernandez, J.M., Machado, A., Chou, R., Riba, J.: CuO, ZrO_2 and ZnO nanoparticles as antiwear additive in oil lubricants. Wear **265**(3–4), 422–428 (2008). doi:10.1016/j.wear.2007.11.013
6. Tenne, R., Redlich, M.: Recent progress in the research of inorganic fullerene-like nanoparticles and inorganic nanotubes. Chem. Soc. Rev. **39**(5), 1423–1434 (2010). doi:10.1039/B901466G
7. Greenberg, R., Halperin, G., Etsion, I., Tenne, R.: The effect of WS_2 nanoparticles on friction reduction in various lubrication regimes. Tribol. Lett. **17**(2), 179–186 (2004). doi:10.1023/B:TRIL.0000032443.95697.1d
8. Eidelman, O., Friedman, H., Rosentveig, R., Moshkovith, A., Perfiliev, V., Cohen, S.R., Feldman, Y., Rapoport, L., Tenne, R.: Chromium-rich coatings with WS_2 nanoparticles containing fullerene-like structure. NANO **6**(4), 313–324 (2011). doi:10.1142/S1793292011002755
9. Redlich, M., Katz, A., Rapoport, L., Wagner, H.D., Feldman, Y., Tenne, R.: Improved orthodontic stainless steel wires coated with inorganic fullerene-like nanoparticles of WS_2 impregnated in electroless nickel-phosphorous film. Dent. Mater. **24**(12), 1640–1646 (2008). doi:10.1016/j.dental.2008.03.030
10. Wu, J.F., Zhai, W.S., Jie, G.F.: Preparation and tribological properties of WS_2 nanoparticles modified by trioctylamine. Proc. Inst. Mech. Eng. Part J **223**(4), 695–703 (2009). doi:10.1243/13506501JET494
11. Wu, J., Zhai, W., Jie, G.: Preparation and tribological properties of tungsten disulfide hollow spheres assisted by methyltrioctylammonium chloride. Tribol. Int. **43**(9), 1650–1658 (2010). doi:10.1016/j.triboint.2010.03.012
12. Hubert, T., Hattermann, H., Griepentrog, M.: Sol-gel-derived nanocomposite coatings filled with inorganic fullerene-like WS_2. J. Sol-Gel. Sci. Technol. **51**(3), 295–300 (2009). doi:10.1007/s10971-009-1896-3
13. Chang, L., Yang, H., Fu, W., Yang, N., Chen, J., Li, M., Zou, G., Li, J.: Synthesis and thermal stability of W/WS_2 inorganic fullerene-like nanoparticles with core-shell structure. Mater. Res. Bull. **41**(7), 1242–1248 (2006). doi:10.1016/j.materresbull.2006.01.019

14. Abate, F., D'Agostino, V., Di Giuda, R., Senatore, A.: Tribological behaviour of MoS_2 and inorganic fullerene-like WS_2 nanoparticles under boundary and mixed lubrication regimes. Tribology **4**(2), 91–98 (2010). doi:10.1179/175158310X12678019274282
15. Rapoport, L., Bilik, Y., Feldman, Y., Homyonfer, M., Cohen, S.B., Tenne, R.: Hollow nanoparticles of WS_2 as potential solid-state lubricants. Nature **387**, 791–793 (1997)
16. Rapoport, L., Feldman, Y., Homyonfer, M., Cohen, H., Sloan, J., Hutchinson, J.L., Tenne, R.: Inorganic fullerene-like material as additives to lubricants: structure-function relationship. Wear **225–229**(2), 975–982 (1999). doi:10.1016/S0043-1648(99)00040-X
17. Cizaire, L., Vacher, B., Le Mogne, T., Martin, J.M., Rapoport, L., Margolin, A., Tenne, R.: Mechanisms of ultra-low friction by hollow inorganic fullerene-like MoS_2 nanoparticles. Surf. Coat. Technol. **160**(2–3), 282–287 (2002). doi:10.1016/S0257-8972(02)00420-6
18. Rapoport, L., Leshchinsky, V., Lapsker, I., Volovik, Y., Nepomnyashchy, O., Lvovsky, M., Popovitz-Biro, R., Feldman, Y., Tenne, R.: Tribological properties of WS_2 nanoparticles under mixed lubrication. Wear **255**(7), 785–793 (2003). doi:10.1016/S0043-1648(03)00044-9
19. Rapoport, L., Nepomnyashchy, O., Lapsker, I., Verdyan, A., Moshkovich, A., Feldman, Y., Tenne, R.: Behaviour of fullerene-like WS_2 nanoparticles under severe contact conditions. Wear **259**(1–6), 703–707 (2005). doi:10.1016/j.wear.2005.01.009
20. Joly-Pottuz, L., Dassenoy, F., Belin, M., Vacher, B., Martin, J.M., Fleischer, N.: Ultralow-friction and wear properties of IF-WS_2 under boundary lubrication. Tribol. Lett. **18**(4), 477–484 (2005). doi:10.1007/s11249-005-3607-8
21. Tevet, O., Von-Huth, P., Popovitz-Biro, R., Rosentsveig, R., Wagner, H.D., Tenne, R.: Friction mechanism of individual multi-layered nanoparticles. Proc. Natl. Acad. Sci. U.S.A., Early Ed. **108**(50), 19901–19906 (2011). doi:10.1073/pnas.1106553108
22. Lahouij, I., Dassenoy, F., de Knoop, L., Martin, J.M., Vacher, B.: In situ TEM observation of the behavior of an individual fullerene-like MoS_2 nanoparticle in a dynamic Contact. Tribol. Lett. **42**, 133–140 (2011)
23. Golan, Y., Drummond, C., Israelachvili, J., Tenne, R.: In situ imaging of shearing contacts in the surface forces apparatus. Wear **245**(1–2), 190–195 (2000). doi:10.1016/S0043-1648(00)00478-6
24. Yadgarov, L., Petrone, V., Rosentsveig, R., Feldman, Y., Tenne, R., Senatore, A.: Tribological studies of rhenium doped fullerene-like MoS_2 nanoparticles in boundary, mixed and elasto-hydrodynamic lubrication conditions. Wear **297**, 1103–1110 (2013)
25. Martin, J.M., Ohmae, N.: Nanoparticles made of metal dichalcogenides. In: Neale, M.J., Priest, M., Stachowiak, G. (eds.) Nanolubricants; Volume 13 of Tribology in Practice Series, pp. 15–40. Wiley, Chichester (2008). doi:10.1002/9780470987711
26. Fang, X., Hua, C., Wu, C., Wang, X., Shen, L., Kong, Q., Wang, J., Hu, Y., Wang, Z., Chen, L.: Synthesis and electrochemical performance of graphene-like WS_2. Chem-Eur. J. **19**(18), 5694–5700 (2013). doi:10.1002/chem.201204254
27. Dumcenco, D.O., Chen, K.Y., Wang, Y.P., Huang, Y.S., Tiong, K.K.: Raman study of 2H-$Mo_{1-x}W_xS_2$ layered mixed crystals. J. Alloys Compd. **506**(12), 940–943 (2010). doi:10.1016/j.jallcom.2010.07.120
28. Ratoi, M., Castle, R.C., Bovington, C.H., Spikes, H.A.: The influence of soot and dispersant on ZDDP film thickness and friction. Lubr. Sci. **17**(1), 25–43 (2004). doi:10.1002/ls.3010170103
29. Aktary, M., McDermott, M.T., McAlpine, G.A.: Morphology and nanomechanical properties of ZDDP antiwear films as a function of tribological contact time. Tribol. Lett. **12**(3), 155–162 (2001)
30. PCS Instruments. MTM (Mini Traction Machine). Retrieved: http://www.pcs-instruments.com/brochures/brochures.shtml#page=page-7
31. Spikes, H.A.: The history and mechanisms of ZDDP. Tribol. Lett. **17**, 465–485 (2004)
32. Ratoi, M., Bovington, C.H., Spikes, H.A.: In situ study of metal oleate friction modifier additives. Tribol. Lett. **14**(1), 33–40 (2003). doi:10.1023/A:1021714231949
33. Xie, F.Y., Gong, L., Liu, X., Tao, Y.T., Zhang, W.H., Chen, S.H., Meng, H., Chen, J.: XPS studies on surface reduction of tungsten oxide nanowire film by Ar + bombardment. J. Electron Spectrosc. Relat. Phenom. **185**(3–4), 112–118 (2012). doi:10.1016/j.elspec.2012.01.004
34. Spath, B., Kopnov, F., Cohen, H., Zak, A., Moshkovich, A., Rapoport, L., Jagermann, W., Tenne, R.: X-ray photoelectron spectroscopy and tribology studies of annealed fullerene-like WS_2 nanoparticles. Phys. Status Solidi B **245**(9), 1779–1784 (2008). doi:10.1002/pssb.200779531
35. Beake, B.D., Zheng, S., Alexander, M.R.: Nanoindentation testing of plasma-polymerised hexane films. J. Mater. Sci. **37**(18), 3821–3826 (2002). doi:10.1023/A:1019626732319
36. Oliver, W.C., Pharr, G.M.: An improved technique for determining hardness and elastic-modulus using load and displacement sensing indentation experiments. J. Mater. Res. **7**(6), 1564–1583 (1992). doi:10.1557/JMR.1992.1564
37. Pereira, G., Lachenwitzer, A., Kasrai, M., Bancroft, G.M., Norton, P.R., Abrecht, M., Gilbert, P.U.P.A., Regier, T., Blyth, R.I.R., Thompson, J.: Chemical and mechanical analysis of tribofilms from fully formulated oils part 1—films on 52100 steel. Tribology **1**(1), 48–61 (2007). doi:10.1179/175158407X189293
38. Bec, S., Tonck, A., Georges, J.M., Roper, G.W.: Synergistic effects of MoDTC and ZDDP on frictional behaviour of tribofilms at the nanometer scale. Tribol. Lett. **17**(4), 797–809 (2004). doi:10.1007/s11249-004-8088-7